41st AIAA/ASME/ASCE/AHS/ASC Structures, Structural Dynamics, and Materials Conference and Exhibit
Atlanta, GA 3-6 April 2000

A00-24575

AIAA-2000-1542

ACTIVE CONTROL OF A PARAMETRICALLY EXCITED STRUCTURAL MODEL OF AN F-15 TAIL SECTION

Ayman A. El-Badawy† and Ali H. Nayfeh‡
Virginia Polytechnic Institute and State University
Blacksburg, Virginia 24061

Abstract

We used a nonlinear control law based on cubic velocity feedback to suppress the vibrations of a structural dynamic model of a twin-tail assembly of an F-15 fighter that is subjected to a principal parametric excitation. The performance of the control law was studied after conducting a stability analysis for the open- and closed-loop responses of the system. Furthermore, we conducted experiments to verify the theoretical analysis using piezoelectric actuators. The theoretical and experimental findings indicate that the control law not only leads to effective vibration suppression, but also to effective bifurcation control.

1.Introduction

Buffeting is defined as the structural response of aircraft structures (such as wings and tails) to unsteady flow[1]. A typical fighter aircraft, such as the F-15, performs maneuvers at high angles of attack (AOA). Depending on the angle of attack and the free stream velocity, vortical flows impinge on the tails and create large dynamic responses, which result in large dynamic loads and stresses throughout the tail structure. These loads may excite different structural modes that cause severe structural fatigue damage and premature structural failure. Thus it is important to reduce the unwanted vibrations caused by buffet loads and thus extend the fatigue life of the F-15 vertical tails.

Several means have been proposed to achieve this goal: (a) passive or active control techniques, (b) reduction of the buffet loads by altering the flowfield around the vertical tails, and (c) changing the load-carrying structure within the tail.

During the ACROBAT (Actively Controlled Response of Buffet Affected Tails) program, Moses[2] used feedback control to the rudder on the starboard fin and to the piezoelectric patches on the port fin. Reductions up to 60 % in the peak value of the PSD of the root bending moment at the frequency of the first bending mode were observed at gains well below the physical limits of the actuators. He noted that the performance of the control law appeared to deteriorate as the AOA was increased. He, also, anticipated that significant improvements in the performance of buffet load alleviation over the entire range of AOA may be achieved by using adaptive control methods that adjust the parameters of the control law based on the AOA.

Moore *et al.*[3] developed a state-space aeroservoelastic model that incorporates 1) a finite element model of the tail structure, 2) an aerodynamic model, which accounts for the aerodynamic inertia damping and stiffness, and 3) a gust disturbance model to replicate the buffet spectrum. The aeroservoelastic model provide the predicted strain levels and accelerations on the tail. An optimization analysis was performed to place the minimum volume of the piezoelectric actuator while maximizing its authority. Finally, a multi-input, multi-output controller was designed using the linear quadratic Gaussian technique. The effective reduction obtained was estimated to be 57% which exceeds their goal of 50%.

Lazarus *et al.*[4] developed a finite element structural model of the F/A 18 vertical tail. They simulated the effect of the piezoelectric actuators on the vertical tail. They developed the unsteady aerodynamic forces using the kernel function method and nonlinear fitting techniques. They analyzed the aerodynamic behavior of the lifting surface by combining the structural model and the aerodynamic model in a state-space representation. They used the available gust disturbance data to include a buffet disturbance model to their overall model. They realized a greater than 50 % reduction in the RMS strain for less than an 8 % increase in the weight of the vertical tail.

Bean *et al.*[5] measured the buffeting response lev-

†Graduate student.

‡University Distinguished Professor, Fellow AIAA.

els on a flexible fin and the unsteady pressure on a rigid fin of similar planform for 60° delta wings with twin fin configurations. They used a laser light sheet visualization technique to determine the vortical flow over the wings. Thus obtained buffeting reductions using tangential leading edge blowing (TLEB). The idea behind TLEB is to inject a thin tangential jet into the cross flow boundary layer near the leading edge and thus enable control of the vortex equilibrium condition at a given AOA. TLEB, therefore, can be considered as a means of reducing the "effective angle of attack" of the vortex. They concluded that a symmetric TLEB at a blowing momentum coefficient of 0.05 induces a linear shift in the buffeting excitation and response. Larger blowing rates can reduce the overall buffet excitation levels and hence substantially reduce the buffeting response levels.

Ferman *et al.*[6] added composite skin doublers or "exoskin" to the main torque box as a mean of stiffness modification. The F-15 stiffness modifications accomplished a 40 % increase in the overall sectional bending stiffness through the use of a precured, cold-bonded, carbon epoxy lay-up. This approach has achieved nearly an order-of-magnitude improvement in fatigue life. Also, selective stiffening of the main torque box by the bond-on exoskin is a simple concept for reducing buffet related vibration and fatigue.

Passive techniques, such as the reinforcement of the structure, can be quite effective and are desirable from the standpoint of simplicity and cost. However, they increase the overall weight of the aircraft, thereby impairing the aircraft's performance. Also, when employed in the F-15 vertical tail, the buffet problem persisted and the cracks were chased from one area to another.

All these papers dealt either with only one tail counting on symmetry or with two tails one rigid and the other flexible. These papers thus missed the interaction between the two tails. According to Ferman *et al.*[6], the structural response characteristics of the left and right vertical tails of the F-15 aircraft are distinctly different. This is primarily due to structural differences in the tip pods, with the left tail being more prone to fatigue than the right tail. Thus, we use a model[7] that allows flexibility of both tails. Also, the model takes into consideration coupling between the two tails. In the experiments, we were able to excite parametrically the twin-tail assembly, hence avoiding any additional masses that might affect the response of the tails.

As it is well-known[8] in the case of parametric excitation, adding damping to the tails will not limit the amplitude of oscillations once the threshold excitation level is exceeded. In fact, adding damping to the tails will only increase the threshold. Consequently, adding damping is not a robust way of controlling the tail vibrations since at high AOA the tails are subjected to extremely high excitation levels. For this reason, we used a nonlinear control law that was developed by Oueini *et al.*[9] to suppress the vibrations of parametrically excited systems. They fedback the cube of the velocity signal to suppress the first mode vibrations of a cantilever beam. We extend their approach by employing a controller for each tail and thus reducing the interaction between the two tails. The maximum response occurs when the excitation frequency is near twice the natural frequency of either of the vertical tails; that is, principal parametric resonance. Thus we use the control law to suppress the tail vibrations at this frequency.

2. Perturbation Solution

The response of the twin-tail assembly to a principal parametric excitation can be modeled by the following two mass normalized second-order coupled differential equations[7]:

$$\ddot{u}_1 + \omega_1^2 u_1 + 2\epsilon\mu_1\dot{u}_1 + \epsilon\alpha_1 u_1^3 + \epsilon\mu_3\dot{u}_1 \mid \dot{u}_1 \mid - \epsilon k(u_2 - u_1) = \epsilon u_1\eta_1 F\cos(\Omega t + \tau_1) + C_1 \quad (1)$$

$$\ddot{u}_2 + \omega_2^2 u_2 + 2\epsilon\mu_2\dot{u}_2 + \epsilon\alpha_2 u_2^3 + \epsilon\mu_4\dot{u}_2 \mid \dot{u}_2 \mid - \epsilon k(u_1 - u_2) = \epsilon u_2\eta_2 F\cos(\Omega t + \tau_2) + C_2 \quad (2)$$

where u_1 and u_2 denote the generalized coordinates of the first bending modes of the twin tail assembly, ω_1 and ω_2 are the lowest linear natural frequencies of the right and left tails, $2\mu_1$and $2\mu_2$ are the linear damping coefficients, α_1 and α_2 are the coefficients of the cubic nonlinearity, μ_3 and μ_4 are the aerodynamic damping coefficients, k is the coupling coefficient of the twin tails, $\eta_1 F u_1\cos(\Omega t + \tau_1)$ and $\eta_2 F u_2\cos(\Omega t + \tau_2)$ are the parametric excitations, η_1 and η_2 are transmissibility terms that make the units of the whole equations consistent, and C_1 and C_2 are the control forces. The parameters in Eqs. (1) and (2) were identified using experimental data[7]. They are listed in Appendix A. We consider a control law given by $C_1 = -\epsilon G_1\dot{u}_1^3$ and $C_2 = -\epsilon G_2\dot{u}_2^3$, where G_1 and G_2 are positive constants. Here ϵ is a bookkeeping parameter, which can be set equal to unity in the final analysis.

To quantitatively describe the nearness of the resonances, we introduce the detuning parameters σ_1 and σ_2 defined by $\Omega = 2\omega_1 + \epsilon\sigma_1$ and $\omega_2 = \omega_1 + \epsilon\sigma_2$. We use the method of multiple scales[10] to generate a first-order approximate solution of Equa-

tions (1) and (2).

$$u_1 = u_{11}(T_0, T_1) + \epsilon u_{12}(T_0, T_1) + \cdots \quad (3)$$

$$u_2 = u_{21}(T_0, T_1) + \epsilon u_{22}(T_0, T_1) + \cdots \quad (4)$$

where $T_0 = t$ is a fast time scale and $T_1 = \epsilon t$ is a slow time scale. In terms of T_0 and T_1, the time derivatives become

$$\frac{d}{dt} = D_0 + \epsilon D_1 + \cdots$$

$$\frac{d^2}{dt^2} = D_0^2 + 2\epsilon D_0 D_1 + \cdots \quad (5)$$

where $D_n = \frac{\partial}{\partial T_n}$. Substituting Eqs. (3)-(5) into Eqs. (1) and (2) and equating coefficients of like powers of ϵ yields

Order 1

$$D_0^2 u_{11} + \omega_1^2 u_{11} = 0 \quad (6)$$
$$D_0^2 u_{21} + \omega_2^2 u_{21} = 0 \quad (7)$$

Order ϵ

$$\begin{aligned} D_0^2 u_{12} + \omega_1^2 u_{12} &= -2D_0 D_1 u_{11} - 2\mu_1 D_0 u_{11} - \alpha_1 u_{11}^3 \\ &+ \eta_1 k_1 (u_{21} - u_{11}) - G_1 (D_0 u_{11})^3 - \mu_3 D_0 u_{11} \\ &\times \mid D_0 u_{11} \mid + \eta_1 u_{11} F \cos(\Omega t + \tau_1) \end{aligned} \quad (8)$$

$$\begin{aligned} D_0^2 u_{22} + \omega_2^2 u_{22} &= -2D_0 D_1 u_{21} - 2\mu_2 D_0 u_{21} - \alpha_2 u_{21}^3 \\ &+ \eta_2 k_2 (u_{11} - u_{21}) - G_2 (D_0 u_{21})^3 - \mu_4 D_0 u_{21} \\ &\times \mid D_0 u_{21} \mid + \eta_2 u_{21} F \cos(\Omega t + \tau_2) \end{aligned} \quad (9)$$

The general solutions of Eqs. (6) and (7) can be written as

$$u_{11} = A_1(T_1) e^{i\omega_1 T_0} + \bar{A}_1(T_1) e^{-i\omega_1 T_0} \quad (10)$$
$$u_{21} = A_2(T_1) e^{i\omega_2 T_0} + \bar{A}_2(T_1) e^{-i\omega_2 T_0} \quad (11)$$

where the $A_i(T_1)$ are determined by eliminating the secular terms from the next-order approximation. Substituting Eqs. (10) and (11) into Eqs. (8) and (9) yields

$$\begin{aligned} D_0^2 u_{12} + \omega_1^2 u_{12} &= -2i\omega_1 A_1' e^{i\omega_1 T_0} - 2\mu_1 i\omega_1 A_1 e^{i\omega_1 T_0} \\ &+ \eta_1 k (A_2 e^{i\omega_2 T_0} - A_1 e^{i\omega_1 T_0}) - \alpha_1 A_1^3 e^{3i\omega_1 T_0} \\ &- 3\alpha_1 A_1^2 \bar{A}_1 e^{i\omega_1 T_0} + \frac{1}{2}\eta_1 F A_1 e^{i\left[(-\Omega+\omega_1)T_0 - \tau_1\right]} \\ &+ \frac{1}{2}\eta_1 F A_1 e^{i\left[(\Omega+\omega_1)T_0 + \tau_1\right]} - \mu_3 [(i\omega_1 A_1 e^{i\omega_1 T_0}) \\ &\times \mid i\omega_1 A_1 e^{i\omega_1 T_0} \mid] - G_1 \Big[- i\omega_1^3 A_1^3 e^{3i\omega_1 T_0} \\ &+ 3i\omega_1^3 A_1^2 \bar{A}_1 e^{i\omega_1 T_0} \Big] + cc \end{aligned} \quad (12)$$

$$\begin{aligned} D_0^2 u_{22} + \omega_2^2 u_{22} &= -2i\omega_2 A_2' e^{i\omega_2 T_0} - 2\mu_2 i\omega_2 A_2 e^{i\omega_2 T_0} \\ &+ \eta_2 k (A_2 e^{i\omega_2 T_0} - A_2 e^{i\omega_2 T_0}) - \alpha_2 A_1^3 e^{3i\omega_2 T_0} \\ &- 3\alpha_2 A_2^2 \bar{A}_2 e^{i\omega_2 T_0} + \frac{1}{2}\eta_2 F A_2 e^{i\left[(-\Omega+\omega_2)T_0 - \tau_2\right]} \\ &+ \frac{1}{2}\eta_2 F A_2 e^{i\left[(\Omega+\omega_2)T_0 + \tau_2\right]} - \mu_4 [(i\omega_2 A_2 e^{i\omega_2 T_0}) \\ &\times \mid i\omega_2 A_2 e^{i\omega_2 T_0} \mid] - G_2 \Big[- i\omega_2^3 A_2^3 e^{3i\omega_2 T_0} \\ &+ 3i\omega_2^3 A_2^2 \bar{A}_2 e^{i\omega_2 T_0} \Big] + cc \end{aligned} \quad (13)$$

Eliminating the terms that produce secular terms in Eqs. (12) and (13) yields

$$\begin{aligned} 2i\omega_1 A_1' + 2\mu_1 i\omega_1 A_1 &= \eta_1 k A_2 e^{i\sigma_2 T_1} - 3\alpha_1 A_1^2 \bar{A}_1 \\ &- \eta_1 k A_1 - i\frac{4}{3\pi}\mu_3 \omega_1^2 a_1^2 e^{i\beta_1} - 3G_1 i\omega_1^3 A_1^2 \bar{A}_1 \\ &+ \frac{1}{2}\eta_1 F(\bar{A}_1) e^{i(\sigma_1 T_1 + \tau_1)} \end{aligned} \quad (14)$$

$$\begin{aligned} 2i\omega_2 A_2' + 2\mu_2 i\omega_2 A_2 &= \eta_2 k A_1 e^{-i\sigma_2 T_1} - 3\alpha_2 A_2^2 \bar{A}_2 \\ &- \eta_2 k A_2 - i\frac{4}{3\pi}\mu_4 \omega_2^2 a_2^2 e^{i\beta_2} - 3G_2 i\omega_2^3 A_2^2 \bar{A}_2 \\ &+ \frac{1}{2}\eta_2 F(\bar{A}_2) e^{i(\sigma_1 T_1 - 2\sigma_2 T_1 + \tau_2)} \end{aligned} \quad (15)$$

Rewriting the A_k in terms of Cartesian coordinates

$$A_k = \frac{1}{2}[p_k(T_1) - iq_k(T_1)] e^{(i\nu_k T_1 + \frac{1}{2}\tau_k)}, \quad k = 1, 2 \quad (16)$$

where

$$\nu_1 = \beta_1' = \frac{1}{2}\sigma_1$$
$$\nu_2 = \beta_2' = \frac{1}{2}\sigma_1 - \sigma_2 \quad (17)$$

and separating Eqs. (14) and (15) into real and imaginary parts, we obtain the modulation equations

$$\begin{aligned} p_1' &= -\frac{4}{3\pi}\mu_3 \omega_1 p_1 \sqrt{p_1^2 + q_1^2} - \frac{1}{2\omega_1}\eta_1 k q_2 + \frac{1}{2\omega_1}\eta_1 k q_1 \\ &+ \frac{3}{8\omega_1}\alpha_1 p_1^2 q_1 + \frac{3}{8\omega_1}\alpha_1 q_1^3 + \frac{\eta_1 F}{4\omega_1} q_1 - \nu_1 q_1 \\ &- \mu_1 p_1 - \frac{3}{8} G_1 \omega_1^2 (p_1^3 + p_1 q_1^2) \end{aligned} \quad (18)$$

$$\begin{aligned} q_1' &= -\frac{4}{3\pi}\mu_3 \omega_1 q_1 \sqrt{p_1^2 + q_1^2} + \frac{1}{2\omega_1}\eta_1 k p_2 - \frac{1}{2\omega_1}\eta_1 k p_1 \\ &- \frac{3}{8\omega_1}\alpha_1 p_1^3 - \frac{3}{8\omega_1}\alpha_1 p_1 q_1^2 + \frac{\eta_1 F}{4\omega_1} p_1 + \nu_1 p_1 \\ &- \mu_1 q_1 - \frac{3}{8} G_1 \omega_1^2 (p_1^2 q_1 + q_1^3) \end{aligned} \quad (19)$$

$$p_2' = -\frac{4}{3\pi}\mu_4\omega_2 p_2\sqrt{p_2^2+q_2^2} - \frac{1}{2\omega_2}\eta_2 k q_1 + \frac{1}{2\omega_2}\eta_2 k q_2 + \frac{3}{8\omega_2}\alpha_2 p_2^2 q_2 + \frac{3}{8\omega_2}\alpha_2 q_2^3 + \frac{\eta_2 F}{4\omega_2}q_2 - \nu_2 q_2 - \mu_2 p_2 - \frac{3}{8}G_2\omega_2^2(p_2^3 + p_2 q_2^2) \quad (20)$$

$$q_2' = -\frac{4}{3\pi}\mu_4\omega_2 q_2\sqrt{p_2^2+q_2^2} + \frac{1}{2\omega_2}\eta_2 k p_1 - \frac{1}{2\omega_2}\eta_2 k p_2 - \frac{3}{8\omega_2}\alpha_2 p_2^3 - \frac{3}{8\omega_2}\alpha_2 p_2 q_2^2 + \frac{\eta_2 F}{4\omega_2}p_2 + \nu_2 p_2 - \mu_2 q_2 - \frac{3}{8}G_2\omega_2^2(p_2^2 q_2 + q_2^3) \quad (21)$$

The performance of the control is evaluated by calculating the equilibrium solutions of Eqs. (18)-(21) and examining their stability as a function of the parameters F, σ_1, and the G_i. We set the time derivatives in Eqs. (18)-(21) equal to zero and solve the resulting system of algebraic equations for p_1, q_1, p_2 and q_2 for a specified value of either σ_1, which is a measure of the detuning of the principal parametric resonance, or F, which is a measure of the forcing amplitude. The amplitudes a_1 and a_2 of the responses of the two tails is then calculated from $a_i = \sqrt{p_i^2 + q_i^2}$. Since there is no closed-form solution for the four algebraic equations, we resorted to numerical techniques. Numerical integration of the modulation equations for different sets of initial conditions was used to locate some of the possible solutions for a given σ_1 and F. Then, starting with these solutions, we used a pseudo arclength scheme[11] to trace the branches of the equilibrium solutions by varying either σ_1 or F.

The stability of a particular equilibrium solution is determined by examining the eigenvalues of the Jacobian matrix of the right-hand sides of Eqs. (18)-(21). If the real part of each eigenvalue is negative, the corresponding equilibrium solution is asymptotically stable. If the real part of any of the eigenvalues is positive, the corresponding equilibrium solution is unstable. In the next two sections, we perform the stability analysis and evaluate the control law.

3. Analytical Force-Response Curves

In Fig. 1, we show the open- and closed-loop force-response curves. First, we consider the open-loop response. When $F < 2.5\ g$, only the trivial solution exists. In the absence of large disturbances, it is maintained as F is increased. When F reaches 3.55 g, the trivial solution looses stability through a subcritical pitchfork bifurcation, and the response amplitude jumps up to the high-amplitude responses in curves (a). A further increase in F leads to a higher response amplitude of the left tail and a lower response amplitude of the right tail. When F is decreased, the response undergoes a saddle-node bifurcation, and the left-tail response jumps down to either another low-amplitude response or the trivial solution. In this region, again the right-tail response amplitude either (a) remains constant (but the phase between the oscillations of the two tails changes) or (b) drops to the trivial solution, depending on the disturbance level.

Second, we consider the response of the closed-loop response. When $G_1 = G_2 = G = 0.01$, the response curves are similar to the uncontrolled response curves. The bifurcations are identical, however, the location of the saddle-node bifurcation is shifted in the case of the right tail and one solution is completely eliminated. On the other hand, for the left tail, the jump-up and jump-down due to the saddle-node bifurcations are eliminated, as shown in curves (b). As the controller gain is further increased, the saddle-node and subcritical pitchfork bifurcations are replaced with one supercritical pitchfork bifurcation at $F = 3.5\ g$. Additionally, the amplitude of the response is further reduced.

4. Analytical Frequency-Response Curves

In Fig. 2, we show the frequency-response curves of the open- and closed-loop system for both the right and left tails. The response amplitudes depend on the value of σ_1 and the system's initial conditions. The solid lines correspond to stable solutions, while the dashed lines correspond to unstable solutions. All of the bifurcations are saddle-node and pitchfork bifurcations. The latter are approximately at the frequencies 19.0 Hz and 21.6 Hz.

We consider first the open-loop response (curves (a) in Fig. 2). The left-tail response is larger than that of the right tail in the frequency range 18.5 till 21.6 Hz. In the frequency range 18.5 Hz till 19.8 Hz, there is another solution where the left-tail response is again larger than the right-tail response. A third solution exists in the frequency range 17.4 Hz to 18.6 Hz where the right-tail response is larger than that of the left tail. We note that the trivial solution loses stability at an excitation frequency of 19.0 Hz through a subcritical pitchfork bifurcation in the forward sweep and at 21.6 Hz in the reverse sweep through a supercritical pitchfork bifurcation.

Next, we consider the response of the closed-loop system. Curves (b-e) all show the responses of both the right and left tails as the controller gain is increased. It is clear that, as the controller gain increases, the response amplitudes of the tails decrease. Also, the bandwidth where the different

responses occur decreases. For example, curve(e), the different coexisting responses in the frequency range 17.3 Hz to 19 Hz are completely eliminated. Also, all of the dangerous subcritical bifurcations are changed to safe supercritical bifurcations and hence the jumps are eliminated.

5. Experiments

The theoretical analysis is verified by implementing the control strategy on the twin-tail assembly fitted with piezoceramic actuators and strain gages. The assembly is excited vertically, thereby subjecting the first modes of the twin tails to a principal parametric resonance.

5.1 Setup and Procedure

The tail section used in the experiments is a 1/16 dynamically scaled model of the F-15 tail assembly. The model was constructed by Professor Sathya Hanagud of the Georgia Institute of Technology from a series of aluminum channels, brass rings, composite plates, metal masses, and various adhesives, as shown in Fig. 3(i). The model is approximately 0.355 m long, 0.228 m tall, and 0.482 m wide.

The tail deflections are measured with a series of four strain gages. The centers of the gage pairs are 0.9 cm and 8.5 cm from the top of the aluminum channels. One pair is on the outside of the right vertical tail; the other pair is on the outside of the left vertical tail. The strain gages are aligned to measure the bending moments. Changes in the gages are measured with a strain gage conditioning amplifier, in a quarter bridge configuration. The actuators used are two patches of the piezoelectric material lead-zirconate-titanate. One patch is installed near the root of each tail. The dimensions of the patches used are $7 \times 3.5 \times .019$ cm.

A series of bolts and several positioning blocks fixes the model to a 250-lb shaker. The shaker excitation is measured with an accelerometer studded to the base. The accelerometer signal is conditioned with an amplifier. The shaker amplifier is driven with a signal generator. The strain gage signal from the conditioner is fed to the controllers, and the nonlinear control signal is generated, amplified, and sent to the actuators. The responses of the tails and the circuit and the accelerometer signals are monitored using a four-channel signal analyzer and an oscilloscope and collected by a data acquisition computer software. Figure 3 (ii) shows the experimental setup.

5.2 Controller Circuit

A hardware controller circuit was built and used with a low-pass filter to generate the cubic velocity signal out of the strain gage signal. The essential components of the circuit includes operational amplifiers (op-amps), two analog multipliers, and other miscellaneous hardware components. The op-amps were used only as buffers between the input and output signals and the circuit, and thus isolate the circuit from the other high-power components. Analog multipliers were utilized to generate the nonlinear term. A chip is connected to perform high-precision (0.1% typical error) 4-quadrant voltage multiplication according to the following relationship:

$$v_{out} = \frac{v_1 - v_2}{v_3 - v_4} \tag{22}$$

where v_{out} is the output voltage of the multiplier and the v_i are the input voltages. Four multipliers are dedicated to the circuit, two for each tail. The remaining circuit components include high-precision potentiometers, metal film resistors, and polystyrene capacitors.

5.3 Location of the Actuators

The goal is to maximize the control authority that can be generated by the actuator; in our case, it is equivelant to maximizing the resultant forces that the actuator develops. Ideally, more actuators would be placed in the areas of high strain than in the areas of low strain. To determine these locations, we glued two strain gages to each tail. One gage at the root and the other at the middle of the tail. Under parametric excitation, we realized that the largest modal response measured by the gage is at the root. Thus we decided to locate the actuators there. It is expected that placing the actuator at any location would stiffen that area and thus reduce the effectiveness of the actuator. However, in our case this is not a problem because the actuator thickness is 1.9 mm. This was confirmed by comparing the force- and frequency-response curves before and after attaching the PZT to the tails. These curves show that the tail dynamics did not change much. For a full scale fighter tail under buffet loads, the actuator placement should be optimized for high performance. Moses[2] provided a good example of such an analysis.

6. Experimental Frequency-Response Curves

We forced the twin-tail assembly at 3.1 g and conducted forward and reverse frequency sweeps. The acceleration of the shaker head was monitored, and the input voltage driving the shaker head was

adjusted to maintain a constant forcing amplitude. In Figs. 4 and 5 , we exhibit the open- and closed-loop frequency-response curves for the right and left tails for both the in-phase and out-of-phase responses.

First, we describe the open-loop case. Initially, as the forcing frequency was increased, the amplitude remained at zero. When the frequency reached a value close to 19.0 Hz for the in-phase response and 17.6 Hz for the out-of-phase, the response jumped up (a subcritical pitchfork bifurcation). We note that for the in-phase response the left-tail response is greater than that of the right tail, while for the out-of-phase response the right tail response is greater than that of the left tail. Further increases in the excitation frequency lead to a decrease in the response amplitudes. When the frequency was approximately 19.5 Hz, the tails stopped oscillating (a supercritical pitchfork bifurcation). Thus, the response remained at zero. In the reverse sweep, the response was similar to that observed during the forward sweep. However, the response amplitude did not experience a jump down at 19.0 Hz in the case of the in-phase response. Instead a growth rate was observed, leading to a very high response amplitude. A jump down to zero occured at 18.5 Hz (a saddle-node bifurcation). For the out-of-phase response, the forward and reverse sweeps were almost similar except that the jump down of the left-tail response occured at a frequency of 18.5 Hz instead of 19.0 Hz, thereby experiencing a large-amplitude response before undergoing a saddle-node bifurcation and jumping down to the trivial response.

Second, we describe the in-phase and out-of-phase frequency-response curves in the closed-loop case . As the forcing frequency was increased, the response remained at zero until the point of subcritical bifurcation where the gain of the controller had to be increased to drive the response to zero. During the reverse sweep, the response amplitude traced the same curve observed during the closed-loop forward sweep. Thus the control law did its job. In fact, we performed another sweep starting with a higher gain and attained a zero-response during the entire sweep.

7. Experimental Force-Response Curves

We forced the twin-tail assembly at a constant frequency of 18.6 Hz and conducted forward and reverse sweeps for both the in-phase and out-of-phase responses. From the experiments, the forward and backward sweeps show similar trends, and thus we only show the forward sweeps in Fig. 6.

First, we describe the open-loop response. As the forcing amplitude was increased, the tails did not oscillate initially. When the forcing amplitude reached approximately 2.85 g in the in-phase case and 2.82 g in the out-of-phase case, the response experienced a jump (a subcritical pitchfork bifurcation) to a high-amplitude response. Further increases in the forcing amplitude lead to an increase in the response amplitude. We note that, at this frequency of excitation, the right-tail response is larger than that of the left tail and vice-versa, depending on the initial condition (the way we pluck the tails).

Second, we examine the closed-loop response. The gains of the controller circuit were chosen to ensure a trivial response of the tails at all excitation levels.

In order to examine the transient characteristics of the control law, we subjected the tails to a forcing level of 3 g and applied control to the worst case scenario of both tails; that is, the right tail was excited at 17.5 Hz and left tail was excited at 18.5 Hz. Figure 7 shows the two time traces for $G_1 = 1$ and $G_2 = 5G_1$. Clearly, increasing the feedback gain resulted in a better transient performance.

8. Conclusions

A nonlinear control law was used to suppress the vibrations of the first bending modes of the twin tails of a 1/16 structural dynamic model of an F-15 twin-tail assembly when subjected to a principal parametric excitation. The dynamics of the first flexural modes of the twin tails were modeled by two second-order coupled nonlinear ordinary-diffferential equations. A control law based on cubic velocity feedback was used. The method of multiple scales was employed to derive four first-order differential equations governing the amplitudes and phases of the response. Then a bifurcation analysis was conducted to examine the stability of the closed-loop system and to investigate the performance of the controller and the effect of the feedback gain on the response. Due to the feedback control law, all of the subcritical pitchfork bifurcations were replaced by safe supercritical ones. The bandwidth of nontrivial solution was reduced, and thus the range of frequencies where the tails can oscillate in high amplitude was reduced. Also, the amplitudes of oscillation of the tails decreased as the gain of the feedback control law increased. Also, increasing the gain improved the transient performance.

We verified the theoretical results with experiments conducted on the structural model of the twin-tail assembly fitted with piezoceramic actuators. An electronic circuit was used to generate the

cubic velocity feedback signal. Good agreement between theory and experiments was obtained.

Acknowledgments

This work was supported by the Air Force Office of Scientific Research under Grant No. F496020-98-1-0393.

References

[1] Mabey, D.G., "Some Aspects of Aircraft Dynamic Loads Due to Flow Separation," *Progress in Aerospace Science,* Vol. 26, 1989, pp. 115-151.

[2] Moses, R.W., "Vertical Tail Buffeting Alleviation Using Piezoelectric Actuators - Some Results of the Actively Controlled Response of Buffet-Affected Tails (ACROBAT) Program." *SPIE's 4th Annual Symposium on Smart Structures and Materials* Vol. 3044, 1997, pp. 87-98.

[3] Moore, J.W., Spangler, R.L., Lazarus, K.B., and Henderson, D.A., "Buffet Load Alleviation Using Distributed Piezoelectric Actuators," in *Proceedings of the ASME Aerospace Division,* Vol. 52, 1996, pp. 485-490.

[4] Lazarus, K.B., Saarmaa, E., and Agnes, G.S., "An Active Smart Material System for Buffet Load Alleviation," *Smart Structures and Integrated Systems* SPIE Vol.2447., 1995, pp. 179-192.

[5] Bean, D. E., and Wood, N.J., "An Experimental Investigation of Twin Fin Buffeting and Suppression", AIAA paper No. 93-0054.

[6] Ferman, M.A., Liguore, S.L., Smith, C.M., and Colvin, B.J., "Composite "Exoskin" Doubler Extends F-15 Vertical Tail Fatigue Life", AIAA paper No. 93-1341-CP.

[7] El-Badawy, A.A., and Nayfeh, A.H., "Nonlinear Identification of a Scaled Structural Dynamic Model of the F-15 Tail Section," in *Proceedings of the 17^{th} International Modal Analysis Conference,* 1999, pp. 1175-1181.

[8] Nayfeh, A.H., and Mook, D.T., *Nonlinear Oscillations,* Wiley, New York, 1979.

[9] Oueini, S.S., and Nayfeh, A.H., "Control of a System Under Principal Parametric Excitation", *The Fourth International Conference on Motion and Vibration Control,* Vol.2, 1998, pp.405-409.

[10] Nayfeh, A.H., *Introduction to Perturbation Techniques,* Wiley, New York, 1981.

[11] Nayfeh, A.H., and Balachandran, B., *Applied Nonlinear Dynamics,* Wiley, New York, 1995.

Appendix A

We estimated the parameters of the model from regressive fits of the experimentally and theoretically determined steady-state response amplitudes. The identified parameters for the right tail are $\zeta_1 = 0.01357$, $\mu_3 = 3.157 \times 10^{-4}\mu\epsilon^{-1}$, $\alpha_1 = -3.675 \times 10^{-2}\frac{1}{s^2\mu\epsilon^2}$, and $\eta_1 = 161.54\frac{1}{gs^2}$. The identified parameters for the left tail are $\zeta_2 = 0.01856$, $\mu_4 = 1.958864 \times 10^{-4}\mu\epsilon^{-1}$, $\alpha_2 = -2.977 \times 10^{-3}\frac{1}{s^2\mu\epsilon^2}$, and $\eta_2 = 275.12\frac{1}{gs^2}$. The estimated value for $k = 87(1/sec^2)$.

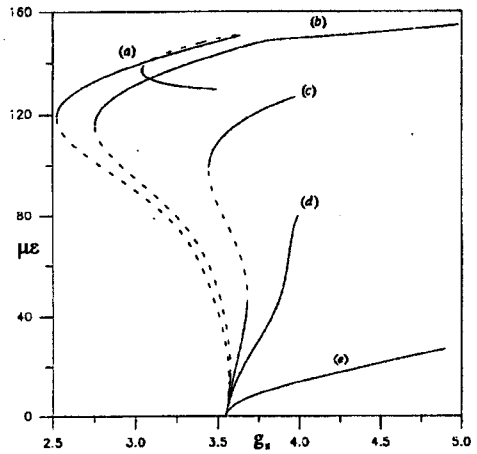

(i) right tail

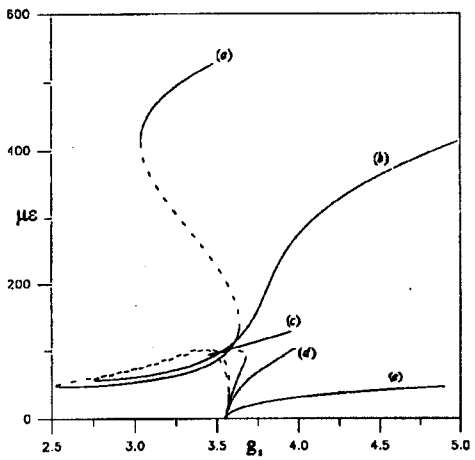

(ii) left tail

Figure 1: Effect of varying the feedback gain on the force-response curves of the specified tail (freq=18 Hz): a) G=0, b) G=0.01, c) G=0.05, d) G=0.1, and e) G=1.

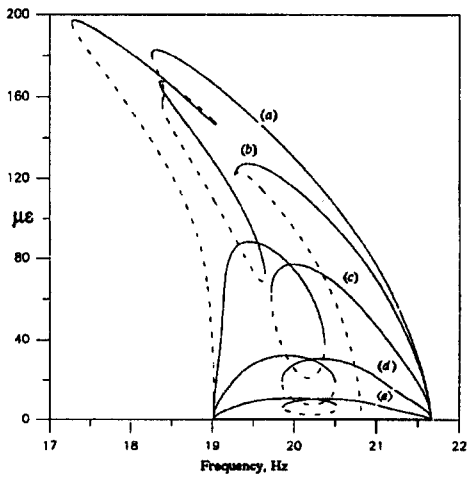

(i) right tail

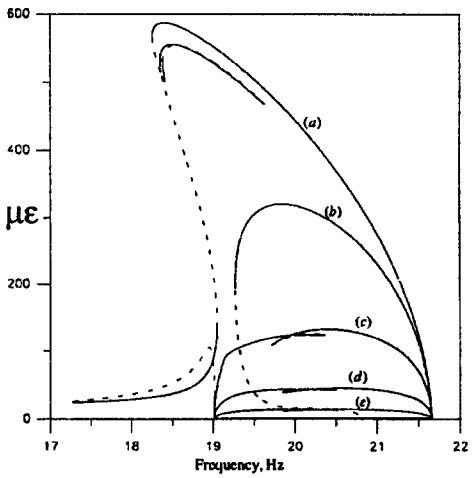

(ii) left tail

Figure 2: Effect of varying the feedback gain on the frequency-response curves of the specified tail (F = 3.2 g): a) G=0, b) G=0.01, c) G=0.1, d) G=1, and e) G=10.

(i)

(ii)

Figure 3: (i) Three-dimensional view of the twin-tail assembly and (ii) experimental setup.

(i) right tail

(ii) left tail

Figure 4: Frequency-response curves of the in-phase responses before and after control.

(i) right tail

(i) inphase responses

(ii) left tail

(ii) out-of-phase responses

Figure 5: Frequency-response curves of the out-of-phase responses before and after control

Figure 6: Force-response curves of the tails before and after control.

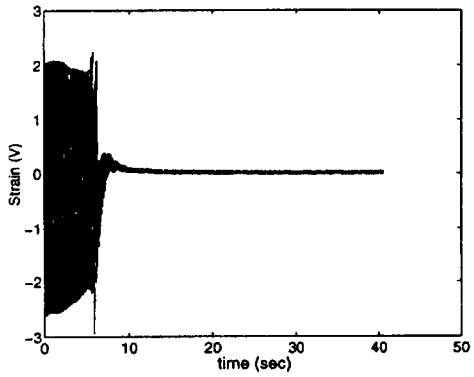

(i) right tail

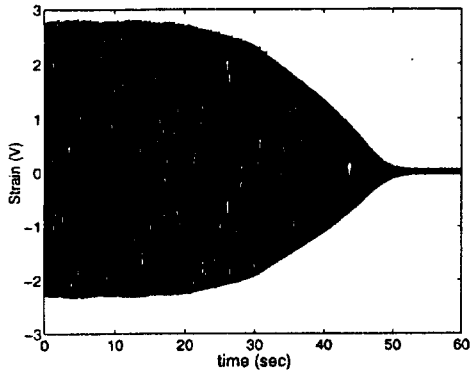

(ii) left tail

Figure 7: Time histories of the responses of the tails before and after applying control for different control gains (a) $G_2 = 5G_1$, and (b) $G_1 = 1$.